heliophilic species than are Central American forests, because the latter suffer more frequent large disturbance events such as severe droughts (*19*). Thus, the flora of BCI, apart from evident biogeographical differences, would have undergone a shift toward heliophily through a more intensive long-term disturbance regime (*20*), and the BCI tree community might have reached a higher degree of species evenness, a situation where any further disturbance could only decrease local species richness, and where recruitment limitation would necessarily play a major role.

Most gap-oriented studies exclude a notable part of the "light level or canopy closure continuum that extends into progressively shadier conditions well beyond the absence of recognizable openings in the forest canopy" (*21, 22*). However, this shadier part of the light gradient is also the result of disturbances: even when they do not result in true canopy opening, the falls of small trees or broken branches modify understory and subcanopy structure, and thus permeability to light. The use of the percentage of heliophilic species as an integrative indirect estimator allowed us to cover the whole range of canopy disturbances in naturally and experimentally disturbed forests.

A premise of the gap paradigm is that the disturbance regime should control species richness exclusively through niche partitioning in recent gaps. However, treefall gaps change the amount and quality of light in the understory not only for a few years, but also for decades after the initial opening. For BCI, Hubbell *et al.* found that "species richness is established very early during gap-phase regeneration." Most tree species of the Guianan forests, many of them locally rare, are more or less shade-tolerant (*18, 23*) and might establish through all phases of gap regeneration. Consequently, species richness is likely to change during mid- and late successional stages as well as very early. The use of a large dbh class allowed us to take into account the cumulative effects of disturbances over a 10-year period.

Hubbell *et al.* (*8*) clearly showed that recruitment limitation is an important phenomenon in the BCI forest tree community. Whereas this is probably true in most tropical rain forests, recruitment limitation does not preclude disturbance regime as a cause of variation in species richness. Our results suggest that %HS can account for more subtle variations in disturbance regimes than the crude measure of recent treefall gaps, and that the intermediate disturbance hypothesis remains a valid explanation for high species diversity in tropical forest trees.

References and Notes

1. J. H. Connell, *Science* **199**, 1302 (1978).
2. E. van der Maarel, *J. Veget. Science* **4**, 733 (1993).
3. For a recent review, see N. L. Brokaw, R. T. Busing, *Trends Ecol. Evol.* **15**, 183 (2000).
4. A. H. Gentry, Ed., *Four Neotropical Rainforests* (Yale Univ. Press, New Haven, CT, 1990).
5. R. Condit, *Trends Ecol. Evol.* **10**, 18 (1995).
6. R. Condit *et al.*, *J. Ecol.* **84**, 549 (1996).
7. N. V. L. Brokaw, *Biotropica* **14**, 158 (1982).
8. S. P. Hubbell *et al.*, *Science* **283**, 554 (1999).
9. Supplementary material is available at www.sciencemag.org/cgi/content/full/294/5547/1702/DC1.
10. L. Schmitt, M. Bariteau, *Bois For. Trop.* **220**, 3 (1990).
11. S. Gourlet-Fleury, F. Houllier, *For. Ecol. Manag.* **131**, 269 (2000).
12. Between October 1986 and January 1988.
13. Trees of dbh (>2800 stems) are monitored yearly. Data are stored in Cirad-forêt's database. We completed them with our own identifications to species.
14. R. L. Chazdon, R. K. Colwell, J. S. Denslow, *Science* **285**, 1459a (1999).
15. S. H. Hurlbert, *Ecology* **52**, 577 (1971).
16. The pertinency of the use of %HS and %PS as disturbance indicators obviously rests on adequate definitions of pioneer and heliophilic species, within a given biogeographical context. For the present study, the reliability of our classification [documented in Supplemental table 2 (9)] and the relevance of both estimators are attested by various tests that we carried out on the Paracou dataset [Supplemental figs. 2 to 6 (9)].
17. In 1994, a 20 m by 500 m transect and a 20 m by 20 m, 100-m apart plot were inventoried for all trees of dbh ≥2 cm. This resulted in 3050 stems (2384 of dbh < 10 cm) in 372 species, including 28 pioneer and 55 heliophilic species. The *terra firme* areas were partitioned into 25 nonoverlapping 20 m by 20 m quadrats.
18. These forests are rich in species with characters reflecting shade tolerance and preference for low levels of disturbance: large seeds, dense wood, and long lifespan (*23*).
19. R. Condit, S. P. Hubbell, R. B. Foster, *J. Trop. Ecol.* **12**, 231 (1996).
20. This postulation is akin to that of J. S. Denslow, *Oecologia* **46**, 18 (1980) [but see (*24, 25*)].
21. M. Lieberman, D. Lieberman, R. Peralta, *Ecology* **70**, 550 (1989).
22. C. D. Canham, *Ecology* **70**, 548 (1989).
23. H. ter Steege *et al.*, *J. Trop. Ecol.* **16**, 801 (2000).
24. T. C. Whitmore, *Biotropica* **16**, 239 (1984).
25. J. S. Denslow, *Biotropica* **16**, 240 (1984).

26. We thank D. Betian, W. Betian, and O. Ngwete for assistance in fieldwork, Cirad-forêt for the use of Paracou database, L. Allorge, B. Holst, P. Maas, S. Mori, O. Poncy, M.-F. Prévost for identifying numerous sterile botanical vouchers, and D. McKey, S. Mori, F. Hallé, M.-F. Prévost, S. Gourlet-Fleury, H. Dessard, and G. Michaloud for valuable comments. This research was granted by the French Ministry of Environment (SOFT Program–GIP ECOFOR).

28 February 2001; accepted 17 September 2001

Identification of Ubiquitin Ligases Required for Skeletal Muscle Atrophy

Sue C. Bodine,[1] Esther Latres,[1] Susanne Baumhueter,[2] Venus K.-M. Lai,[1] Lorna Nunez,[1] Brian A. Clarke,[1] William T. Poueymirou,[1] Frank J. Panaro,[1] Erqian Na,[1] Kumar Dharmarajan,[1] Zhen-Qiang Pan,[3] David M. Valenzuela,[1] Thomas M. DeChiara,[1] Trevor N. Stitt,[1] George D. Yancopoulos,[1] David J. Glass[1]*

Skeletal muscle adapts to decreases in activity and load by undergoing atrophy. To identify candidate molecular mediators of muscle atrophy, we performed transcript profiling. Although many genes were up-regulated in a single rat model of atrophy, only a small subset was universal in all atrophy models. Two of these genes encode ubiquitin ligases: *Muscle RING Finger 1* (*MuRF1*), and a gene we designate *Muscle Atrophy F-box* (*MAFbx*), the latter being a member of the SCF family of E3 ubiquitin ligases. Overexpression of *MAFbx* in myotubes produced atrophy, whereas mice deficient in either *MAFbx* or *MuRF1* were found to be resistant to atrophy. These proteins are potential drug targets for the treatment of muscle atrophy.

Muscle atrophy occurs as a consequence of denervation, injury, joint immobilization, bed rest, glucocorticoid treatment, sepsis, cancer, and aging (*1*). Unfortunately, there are no effective treatments for muscle atrophy. The maintenance of muscle mass is controlled by a balance between protein synthesis and protein degradation pathways, which is thought to shift toward protein degradation during atrophy (*1*). Recently, a signaling pathway that increases protein synthesis was shown to promote muscle hypertrophy, thereby overcoming muscle atrophy (*2*, *3*). Although protein degradation systems have been extensively studied, specific molecular mediators of at-

[1]Regeneron Pharmaceuticals, 777 Old Saw Mill River Road, Tarrytown, NY, 10591–6707, USA. [2]Applied Biosystems, 850 Lincoln Center Drive, Foster City, CA 94404, USA. [3]Derald H. Ruttenberg Cancer Center, Mount Sinai School of Medicine, New York, NY, 10029–6574, USA.

*To whom correspondence should be addressed. E-mail: david.glass@regeneron.com

rophy-related degradation have not been defined, nor has it been demonstrated whether blocking such specific mediators can inhibit muscle atrophy. Further, it is unknown whether muscle atrophy caused by disparate perturbations is controlled by a common signaling pathway or whether distinct pathways can lead to muscle wasting.

Denervation, immobilization, and unweighting in rats all result in similar rates of loss in mass of the medial gastrocnemius muscle, a result which is consistent with the idea that there are common mechanisms leading to atrophy (Fig. 1A). To identify potential universal markers of atrophy, we attempted to identify genes regulated in immobilization, and then determined which of these were similarly regulated in multiple other models. We first compared mRNA from rat medial gastrocnemius muscle that had been immobilized for 3 days to mRNA from control muscle, via the GeneTag differential display approach (*4*). We analyzed a relatively early time point (3 days) to identify genes that may function as potential triggers, as well as markers, of the atrophy process. Only genes whose expression changed by threefold or more were accepted as being differentially regulated. Seventy-four transcripts were identified (*4*) and then assayed for universality by Northern analysis using panels of mRNA prepared from muscle subjected to denervation, immobilization, or unweighting for periods of 1 to 14 days.

Although most genes perturbed during immobilization were similarly regulated during denervation, most of these genes were unaltered in the unweighting model, despite the fact that similar rates of atrophy were seen in these models (Fig. 1A). Two genes, however, were identified that were up-regulated in all three models of atrophy: *MuRF1* (for Muscle RING Finger 1) and *MAFbx* (for Muscle Atrophy F-box) (Fig. 1B).

MuRF1 and *MAFbx* expression were analyzed in two additional models of skeletal muscle atrophy: treatment with the cachectic cytokine interleukin-1 (IL-1) (*5*) and treatment with the glucocorticoid dexamethasone (*6*). Both cachectic agents caused an up-regulation of *MuRF1* and *MAFbx*, with dexamethasone resulting in a greater than 10-fold increase in expression of both genes (Fig. 1C). Analysis of rat and human tissues revealed that *MuRF1* and *MAFbx* mRNAs were expressed selectively in cardiac and skeletal muscle (Fig. 1D), which is consistent with their serving specific roles in these tissues.

Because *MAFbx* had not been previously identified, we cloned full-length rat and human cDNAs for this gene. Open reading frames of rat and human *MAFbx* cDNA sequence predict proteins that are 90% identical (*4*). MAFbx contains an F-box domain, which is characteristic of proteins that are components of a particular type of E3 ubiquitin ligase called an SCF ubiquitin-ligase complex (*7*, *8*). The SCF complex is thus named because it involves stable interactions between Skp1, Cullin1, and one of many F-box–containing proteins (Fbps). More than 38 different Fbps have been identified in humans (*9*, *10*), with the closest relative to MAFbx being Fbx25 (*10*). Two lines of evidence indicate that MAFbx is in fact an SCF-type E3 ubiquitin ligase. First, yeast two-hybrid cloning using full-length MAFbx as a "bait" resulted in 94 independent clones of Skp1, out of a total of 94 clones obtained in the interaction experiment (*11*). Second, affinity purification of MAFbx from mammalian cells transfected with *MAFbx* resulted in the copurification of both endogenous Skp1 and Cullin1 (Fig. 2A). This copurification was dependent on the presence of the F-box domain in MAFbx (Fig. 2A, compare lanes 3 and 4). The F-box motif has been shown to be necessary for interaction between Fbps and Skp1 (*12*).

To determine whether *MAFbx* expression was sufficient to cause muscle atrophy, we generated an adenovirus encoding rat *MAFbx* and *Enhanced Green Fluorescent Protein* (*EGFP*) (*13*). We then infected differentiated, postmitotic, multinucleated C2C12 skeletal myotubes (*14*) with either a control adenovirus expressing *EGFP* alone or a *MAFbx-EGFP* expressing adenovirus (in which myc-tagged *MAFbx* was coexpressed with *EGFP*, via an internal ribosomal entry sequence). After 2 days, the

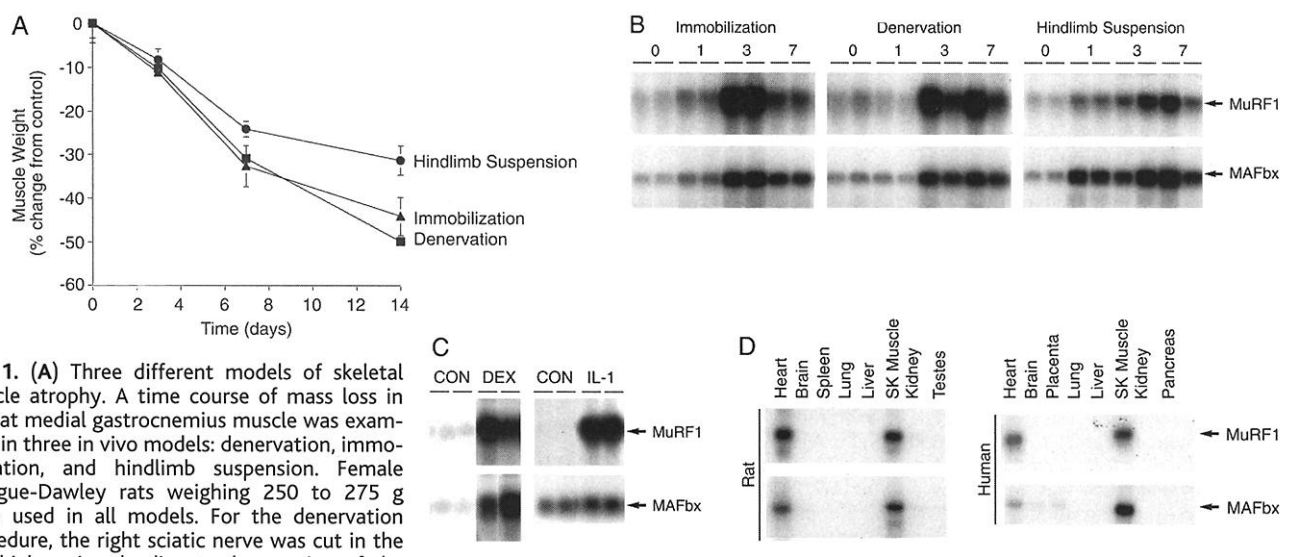

Fig. 1. (**A**) Three different models of skeletal muscle atrophy. A time course of mass loss in the rat medial gastrocnemius muscle was examined in three in vivo models: denervation, immobilization, and hindlimb suspension. Female Sprague-Dawley rats weighing 250 to 275 g were used in all models. For the denervation procedure, the right sciatic nerve was cut in the midthigh region, leading to denervation of the lower limb muscles. For the immobilization procedure, the right ankle joint was fixed at 90° of flexion by insertion of a screw (1.2 × 8 mm) through the calcaneous and talis into the shaft of the tibia. For the hindlimb suspension procedure, the hindlimbs were unloaded by suspending the rats by their tails with a tail-traction bandage as described (*18*). On the indicated days, rats were killed and hindlimb muscles were removed, weighed, and frozen. Weight-matched untreated rats served as controls. Data are means ± SEM, $n = 10$ rats. (**B**) Northern blots (*4*) showing the effect of atrophy on *MuRF1* and *MAFbx* transcripts. Medial gastrocnemius muscle was obtained from rats undergoing a time course (0, 1, 3, and 7 days) of three atrophy models: ankle-joint immobilization, denervation, and hindlimb suspension. (**C**) Northern blots (*4*) showing the effect of dexamethasone (DEX) and IL-1 on expression of *MuRF1* and *MAFbx*. Medial gastrocnemius muscle was obtained from untreated rats (CON) and from rats treated with DEX, delivered orally at a concentration of 6 μg/ml for 9 days, and from rats treated with IL-1, delivered subcutaneously daily at a dose of 0.1 mg per kilogram of body weight for 3 days. (**D**) Tissue-specific expression of *MuRF1* and *MAFbx*. SK, skeletal. mRNA obtained from rat and human tissues (Clontech) was hybridized with probes for the indicated genes (*4*).

myotubes expressing the *MAFbx* gene were significantly thinner than the *EGFP*-infected cells, as determined by measuring myotube diameter (Fig. 2B). An immunoblot of protein lysates with an antibody to EGFP allowed for a relative determination of infection levels in *EGFP* and *MAFbx-EGFP* cultures (Fig. 2C). Immunoblotting with an antibody to the MAFbx myc-epitope tag confirmed the production of MAFbx protein in the *MAFbx*-infected myotubes (Fig. 2C).

The RING finger protein MuRF1 was previously identified by virtue of its interaction in a yeast two-hybrid experiment with a domain of the sarcomeric protein titin (*15*). MuRF1 contains all the canonical structural features of RING-domain–containing monomeric ubiquitin ligases (*16*, *17*). After confirming that MuRF1 protein levels increased during atrophy (*4*), we tested recombinant MuRF1 protein for ubiquitin ligase activity in an in vitro assay. MuRF1 was required for the formation of a high-molecular-weight ubiquitin polymer, indicating that it functions as a ubiquitin ligase (Fig. 2D).

To investigate the in vivo function of *MAFbx* and *MuRF1*, we genetically engineered mice with null alleles for these genes. For *MAFbx*, a specific gene deletion was generated by replacing the genomic DNA spanning the ATG through the exon encoding the F-box region with a *LacZ/neomycin* cassette (*4*). For *MuRF1*, genomic DNA spanning the ATG through the fifth exon was replaced with a *LacZ/neomycin* cassette (*4*). The addition of the *LacZ* cassette in each case allowed us to simultaneously disrupt gene function and perform β-galactosidase (β-Gal) staining to determine gene expression patterns. Analysis of the genetic loci demonstrated the expected perturbations in *MAFbx* (Fig. 3A) and *MuRF1* (Fig. 3C) +/– and –/– mice. Further, $MAFbx^{-/-}$ mice were null for *MAFbx* mRNA (Fig. 3B), and $MuRF1^{-/-}$ mice were null for *MuRF1* mRNA (Fig. 3D). Both $MAFbx^{-/-}$ and $MuRF1^{-/-}$ mice were viable and fertile and appeared normal. Knockout mice had normal growth curves relative to those of wild-type litter mates, and skeletal muscles and the heart had normal weights and morphology.

We then challenged the mice in an atrophy model to determine the effect of MAFbx

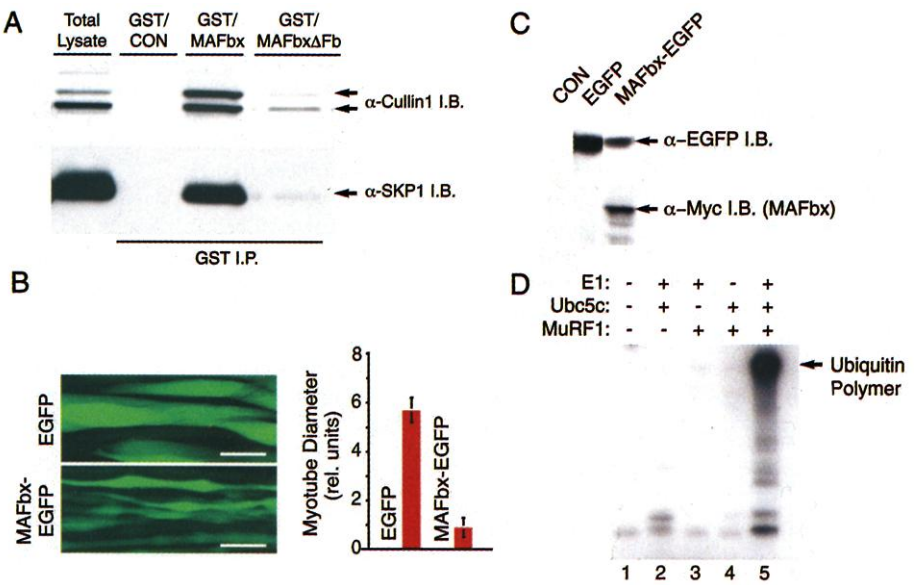

Fig. 2. (**A**) MAFbx interacts with the SCF complex components Cullin1 and Skp1. Vectors encoding glutathione *S*-transferase (GST) (GST/CON), GST-MAFbx, or GST-MAFbxΔFb (an F-box deletion of MAFbx, amino acids 216 through 263) were transiently transfected into Cos7 cells (*4*). Both Cullin1 and Skp1 could be copurified, with glutathione-agarose beads, from lysates of cells transfected with GST-MAFbx (lane 3). Deletion of the F box markedly reduced the amount of Cullin1 and Skp1, which coprecipitated (lane 4). I.B., immunoblot. (**B**) Overexpression of MAFbx causes atrophy. C2C12 myotubes were either uninfected (CON) or infected with an adenovirus expressing *EGFP*, or with an adenovirus expressing both a Myc-epitope–tagged rat *MAFbx* gene and *EGFP* (MAFbx-EGFP). At day 4 after differentiation, fluorescent myotubes were photographed, and myotube diameters were measured (right). The adenoviruses were generated as described (*13*). Calibration = 50 μm. (**C**) Determination of infection levels. Because the EGFP and MAFbx-EGFP viruses contained the *EGFP* gene, an anti-EGFP immunoblot allowed for a relative determination of infection levels (top). An immunoblot of lysates confirmed the presence of Myc-epitope–tagged MAFbx protein in the myotubes infected with the MAFbx virus (bottom). (**D**) MuRF1 protein has ubiquitin ligase activity. Purified glutathione-Sepharose–bound MuRF1 protein (GST-MuRF1) was added to a ubiquitin ligase reaction as described (*19*). Briefly, recombinant GST-MuRF1 (100 ng) was incubated with ^{32}P-labeled ubiquitin (3 μg) in the presence of ATP, E1, and recombinant Ubc5c (lane 5). In lanes 1 through 4, indicated components were omitted. Aliquots of the reaction were analyzed by 12.5% SDS-polyacrylamide gel electrophoresis to detect ^{32}P-labeled high-molecular-weight ubiquitin conjugates. The "ubiquitin polymer" may include ubiquitinated Ubc5c and MuRF1.

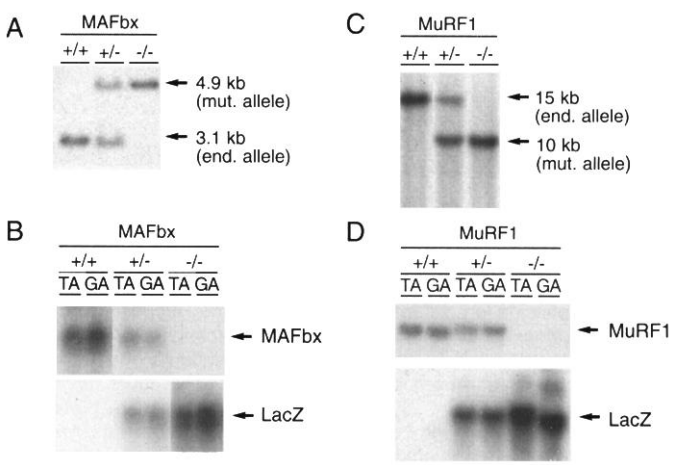

Fig. 3. (**A**) The targeting of the *MAFbx* gene was confirmed in embryonic stem (ES) cells and in both heterozygous and homozygous *MAFbx* mutant mice by digestion of genomic tail DNA with Eco RI and probing with a 5′ 1.1-kb Sac II fragment to detect the endogenous (end. allele) 3.1-kb and targeted (mut. allele) 4.9-kb Eco RI fragments (*4*). (**B**) The targeted mutation in the *MAFbx* gene was verified by probing mRNA from both tibialis anterior (TA) and gastrocnemius (GA) muscle prepared from *MAFbx* +/+, +/–, and –/– mice with a *MAFbx* probe, spanning base pairs (bp) 660 through 840 of coding sequence (*MAFbx*, upper panel), as well as with a probe of the inserted *LacZ* gene (lower panel). (**C**) The targeting of the *MuRF1* gene was confirmed in ES cells and in both heterozygous and homozygous *MuRF1* mutant mice by digestion of genomic tail DNA with Eco RI and probing with a 5′ 0.5-kb Bgl II fragment to detect the endogenous (end. allele) 15-kb and targeted (mut. allele) 10-kb Eco RI fragments (*4*). (**D**) The targeted mutation in the *MuRF1* gene was verified by probing mRNA from both TA and GA muscle prepared from *MuRF1* +/+, +/–, and –/– mice with a probe spanning bp 1 through 500 of rat *MuRF1* coding sequence (*MuRF1*, upper panel), as well as with a probe of the inserted *LacZ* gene (lower panel).

and MuRF1 deficiency on skeletal muscle loss. Muscle atrophy was induced by cutting the sciatic nerve, resulting in denervation and disuse of the tibialis anterior and gastrocnemius muscles. Denervation resulted in the up-regulation of *LacZ* expression from the *MAFbx* and *MuRF1* gene loci in all muscle fibers, as demonstrated by β-Gal staining in the tibialis anterior muscle of heterozygous *MAFbx* and *MuRF1* mice (Fig. 4A). Wild-type mice had significant muscle atrophy in the gastrocnemius muscles at 7 and 14 days after denervation (Fig. 4B). In contrast, the $MAFbx^{-/-}$ mice had significant muscle sparing relative to $MAFbx^{+/+}$ mice at both 7 and 14 days (Fig. 4B). At 14 days, the $MAFbx^{-/-}$ mice exhibited a 56% sparing of muscle as compared with the wild-type mice. $MAFbx^{-/-}$ mice exhibited no additional muscle loss between 7 and 14 days, whereas $MAFbx^{+/+}$ mice continued to lose mass. The sparing of muscle mass at 14 days was also reflected in a preservation of mean fiber size and fiber size variability; $MAFbx^{-/-}$ mice had significantly larger fibers than did the $MAFbx^{+/+}$ mice, and muscle in the denervated limb had the same fiber size variability (standard deviation) as that in the control limb (wild type versus knockout: control, 2146 ± 375 μm² versus 2053 ± 420 μm²; denervated, 1068 ± 122 μm² versus 1508 ± 284 μm²) (Fig. 4C).

The $MuRF1^{-/-}$ mice also had significant muscle sparing at 14 days of denervation but not at 7 days (Fig. 4B). At 14 days, the $MuRF1^{-/-}$ exhibited a 36% sparing of muscle as compared with the wild-type (+/+) mice. These data provide strong evidence that both MAFbx and MuRF1 are critical regulators of muscle atrophy, most likely through the regulation of the degradation of crucial muscle proteins.

The discovery of two ubiquitin ligases as markers for multiple models of skeletal muscle atrophy suggests that highly disparate perturbations, ranging from denervation to glucocorticoid treatment, activate common atrophy-inducing pathways. Further, the particular function of ubiquitin ligases—to target discrete substrates for proteolysis by the adenosine triphosphate (ATP)–dependent proteasome—suggests that either a single protein degradation pathway is up-regulated during atrophy, which requires both MAFbx and MuRF1; or that parallel pathways in which these genes play required roles are up-regulated.

Because both *MuRF1* and *MAFbx* are also specifically expressed in cardiac muscle, it will be important to examine the roles of these ubiquitin ligases in heart remodeling and disease and to determine whether loss of either *MuRF1* or *MAFbx* affects cardiac function. The current studies identify *MuRF1* and *MAFbx* as markers of skeletal muscle atrophy and potential targets for therapeutic intervention to prevent the loss of skeletal muscle in clinical settings of atrophy.

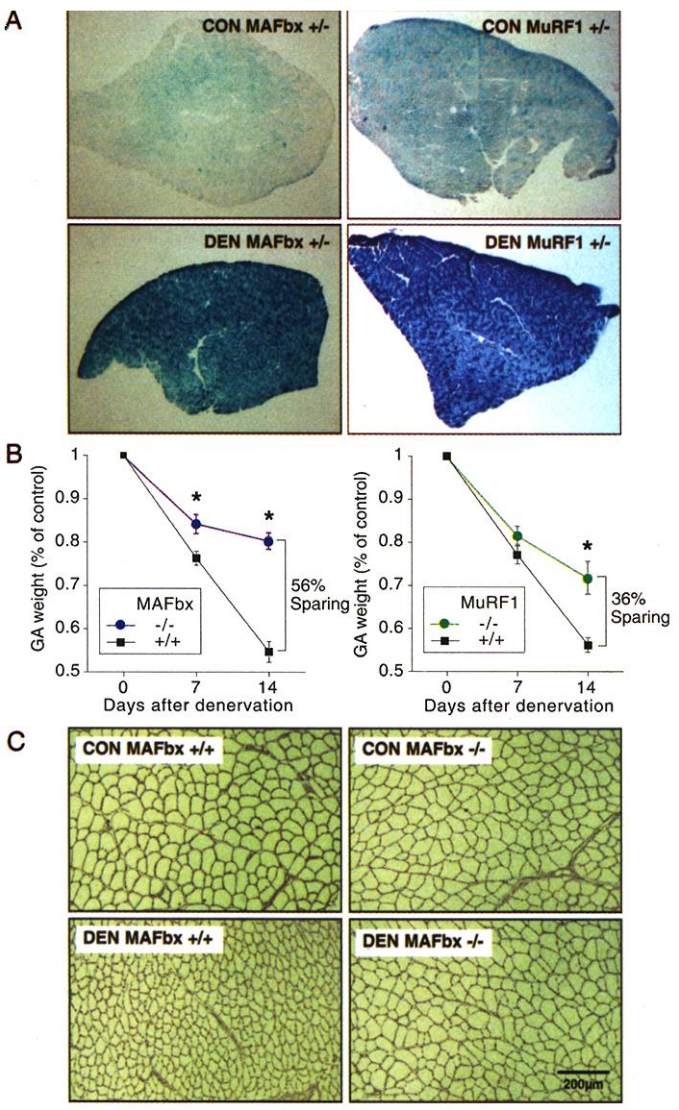

Fig. 4. **(A)** The *MAFbx* and *MuRF1* genes are up-regulated in muscle after denervation. The regulation of the *MAFbx* and *MuRF1* genes was examined with β-Gal staining in $MAFbx^{+/-}$ and $MuRF1^{+/-}$ mice. The right sciatic nerve was cut in heterozygous mice, resulting in denervation of the TA muscle. Seven days later, the right and left TA muscles were sectioned and stained for β-Gal activity, in the same media, for equivalent times. In control muscle, there is a low level of *MAFbx* expression in some (primarily deep region), but not all, muscle fibers of the TA muscle. In comparison, *MuRF1* is expressed in all fibers at a slightly higher level than *MAFbx*. After denervation, both *MAFbx* and *MuRF1* expression are up-regulated in all muscle fibers. **(B)** Muscle from *MAFbx*- and *MuRF1*- deficient mice maintains muscle mass after denervation, as compared to that of wild-type (+/+) mice. The right hindlimb muscles of adult mice (*MAFbx* +/+ and –/–) were denervated by cutting the right sciatic nerve. The left hindlimb of each animal served as its own control. At 7 and 14 days after denervation, the right and left GA muscle complex was removed and weighed. Muscle weights (GA) are plotted as a percent of control, calculated as the right/left muscle weights. Data are means ± SEM, n = 5 to 10 mice. **(C)** Muscle fiber size and variability were maintained in muscles from *MAFbx*-deficient mice after denervation. Cross sections taken from the TA muscle were stained with an antibody against laminin (Sigma). Representative cross sections are shown from the TA muscle: wild type (+/+), control left side (upper left); wild type (+/+), 14-day-denervated (DEN) right side (lower left); homozygous (–/–), control left side (upper right); homozygous, 14-day-denervated right side (lower right).

References and Notes

1. R. T. Jagoe, A. L. Goldberg, *Curr. Opin. Clin. Nutr. Metab. Care* **4**, 183 (2001).
2. C. Rommel *et al.*, *Nature Cell Biol.* **3**, 1009 (2001).
3. S. C. Bodine *et al.*, *Nature Cell Biol.* **3**, 1013 (2001).
4. Additional data and methods used in this study are described in the supplementary Web material, available on *Science* Online at www.sciencemag.org/cgi/content/full/1065874/DC1. GenBank accession numbers are as follows: rat *MAFbx*, AY059628; human *MAFbx*, AY059629; and rat *MuRF1*, AY059627. For Northern methods and probe details, ref. (*2*) of Web material. Knockouts were done with the proprietary Velocigene technology, which allows for the rapid and high-throughput generation of custom gene mutations in mice (T. M. De Chiara, W. T. Poueymirou, D. M. Valenzuela, G. D. Yancopoulos, unpublished data).
5. R. N. Cooney, S. R. Kimball, T. C. Vary, *Shock* **7**, 1 (1997).
6. A. L. Goldberg, *J. Biol. Chem.* **244**, 3223 (1969).
7. D. Skowyra, K. L. Craig, M. Tyers, S. J. Elledge, J. W. Harper, *Cell* **91**, 209 (1997).
8. J. Lisztwan *et al.*, *EMBO J.* **17**, 368 (1998).
9. J. T. Winston, D. M. Koepp, C. Zhu, S. J. Elledge, J. W. Harper, *Curr. Biol.* **9**, 1180 (1999).
10. C. Cenciarelli *et al.*, *Curr. Biol.* **9**, 1177 (1999).
11. L. Nunez, D. J. Glass, unpublished data.
12. E. T. Kipreos, M. Pagano, *Genome Biol.* **1**, 3002.1 (2000).

13. T.-C. He *et al.*, *Proc. Natl. Acad. Sci. U.S.A.* **95**, 2509 (1998).
14. W. Bains, P. Ponte, H. M. Blau, L. Kedes, *Mol. Cell. Biol.* **4**, 1449 (1984).
15. T. Centner *et al.*, *J. Mol. Biol.* **306**, 717 (2001).
16. P. S. Freemont, *Curr. Biol.* **10**, R84 (2000).
17. C. A. Joaeiro, A. M. Wiessman, *Cell* **102**, 549 (2000).
18. D. B. Thomason, R. E. Herrick, D. Surdyka, K. M. Baldwin, *J. Appl. Physiol.* **63**, 130 (1987).
19. A. Chen *et al.*, *J. Biol. Chem.* **275**, 15432 (2000).
20. We thank L. S. Schleifer and P. R. Vagelos for their enthusiastic support; E. Burrows, B. Efraim, and V. Lan for expert graphics work; and M. Gonzalez for insightful discussions. We thank members of the Muscle in vivo and in vitro groups, transgenic group, and tissue culture group for their expert technical assistance.

30 August 2001; accepted 17 October 2001
Published online 25 October 2001;
10.1126/science.1065874
Include this information when citing this paper.

Taking Cell-Matrix Adhesions to the Third Dimension

Edna Cukierman, Roumen Pankov, Daron R. Stevens, Kenneth M. Yamada*

Adhesions between fibroblastic cells and extracellular matrix have been studied extensively in vitro, but little is known about their in vivo counterparts. Here, we characterized the composition and function of adhesions in three-dimensional (3D) matrices derived from tissues or cell culture. "3D-matrix adhesions" differ from focal and fibrillar adhesions characterized on 2D substrates in their content of $\alpha_5\beta_1$ and $\alpha_v\beta_3$ integrins, paxillin, other cytoskeletal components, and tyrosine phosphorylation of focal adhesion kinase (FAK). Relative to 2D substrates, 3D-matrix interactions also display enhanced cell biological activities and narrowed integrin usage. These distinctive in vivo 3D-matrix adhesions differ in structure, localization, and function from classically described in vitro adhesions, and as such they may be more biologically relevant to living organisms.

Our current understanding of cell-matrix adhesions—the cell surface structures that mediate cell interactions with extracellular matrix (ECM)—is based primarily on in vitro studies of focal adhesions and other adhesive structures, particularly in fibroblasts (*1–4*). Focal adhesions are integrin-based structures that mediate strong cell-substrate adhesion and transmit information in a bidirectional manner between extracellular molecules and the cytoplasm (*1–7*). A second structure termed the fibrillar adhesion (*8*) functions in generating extracellular fibrils of fibronectin (*9*). Our knowledge about the roles of these structures in cell adhesion, migration, signaling, and cytoskeletal function is derived primarily from studies on planar 2D tissue culture substrates. However, the importance of 3D ECM is recognized for epithelial cells, where 3D environments promote normal epithelial polarity and differentiation (*10*). Fibroblastic cells have been studied mainly in 2D cell cultures, yet culturing them on flat substrates induces an artificial polarity between the lower and upper surfaces of these normally nonpolar cells; not surprisingly, fibroblast morphology and migration differ once suspended in collagen gels (*11, 12*). Relatively little is known about the cell-matrix adhesive structures formed in 3D matrices of living tissues, particularly in the natural in vivo environments of migrating cells during embryonic development.

Using current knowledge about the molecular composition and functions of the in vitro cell-matrix adhesions formed by fibroblasts, we searched for comparable structures in 3D environments. In 2D cell culture, focal and fibrillar adhesions have distinct molecular compositions: Focal ad-

Craniofacial Developmental Biology and Regeneration Branch, National Institute of Dental and Craniofacial Research, National Institutes of Health, Bethesda, MD 20892, USA.

*To whom correspondence should be addressed. E-mail: ky4w@nih.gov

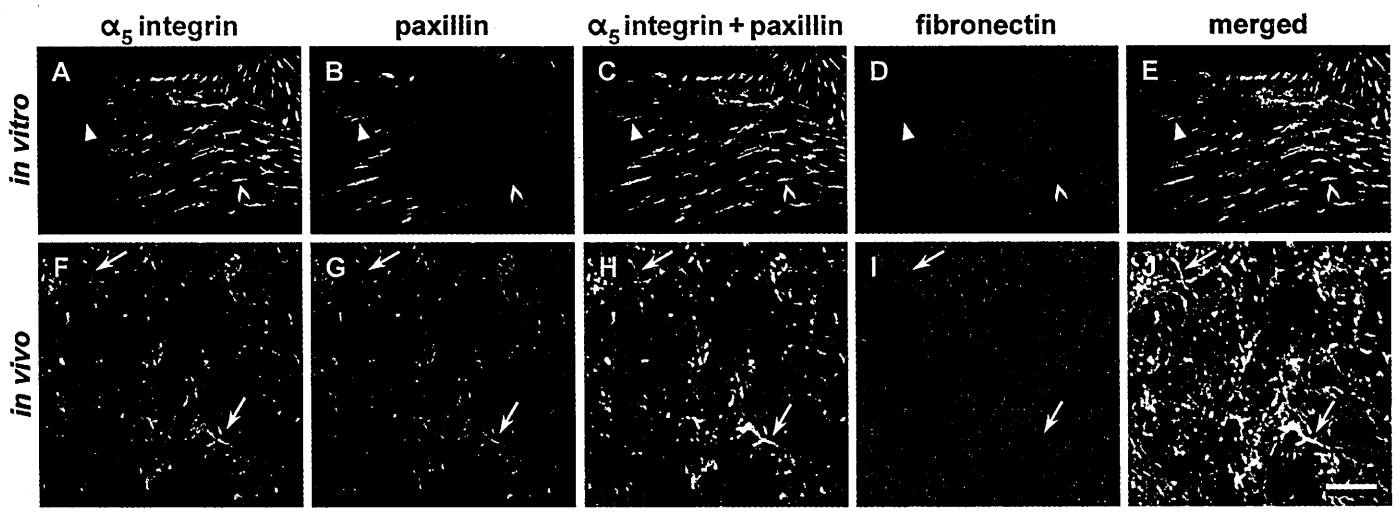

Fig. 1. In vivo 3D-matrix adhesions differ from focal or fibrillar adhesions on 2D substrates. (**A** to **E**) Confocal images of indirect immunofluorescence staining of an NIH-3T3 mouse fibroblast in vitro on a 2D fibronectin-coated cover slip; (**F** to **J**) transverse cryostat craniofacial mesenchyme sections of an E13.5 mouse embryo. α_5 integrin [(A) and (F), green] and paxillin [(B) and (G), red] colocalize in a fibrillar organization in mesenchymal tissue [(H), yellow in merged image indicates overlap of red and green labels], but not on a 2D substrate in vitro (C). Fibronectin [(D) and (I), blue] localizes to fibrillar structures in vivo, and merged images indicate substantial overlap of all three molecules [(J), white compared to (E)]. Note that focal adhesions (filled arrowheads) and fibrillar adhesions (open arrowheads) show differential localization of the α_5 integrin and paxillin markers only on traditional flat 2D substrates in vitro. The 3D-matrix adhesions (arrows) identified by triple localization are present in 3D environments in vivo. Scale bar, 5 μm.